

Optimised Least Squares Approach for Accurate Rectangle Fitting

Yiming Quan^{a,b,*}, Shian Chen^a

^a*Ningbo Tianyi Design Research of Surveying and Mapping Co. Ltd, 2F Huashang Mansion, No 100 Xinghai South Road, Ningbo, 315040, Zhejiang, China*

^b*Department of Civil Engineering, Engineering College, Lishui University, No 1 Xueyuan Road, Lishui, 323000, Zhejiang, China*

Abstract

This study presents a novel and efficient least squares based method for rectangle fitting, using a continuous fitness function that approximates a unit square accurately. The proposed method is compared with the existing method in the literature using both simulated data and real data. The real data is derived from aerial photogrammetry point clouds of a rectangular building. The simulated tests show that the proposed method performs better than the reference method, reducing the root-mean-square error by about 93% and 14% for clean datasets and noisy point clouds, respectively. The proposed method also improves the fitting of the real dataset by about 81%, achieving centimetre level accuracy. Furthermore, the test results show that the proposed method converges in fewer than 10 iterations.

Keywords: Rectangle fitting, Least squares, Gauss-Newton, Rectangle parameter estimation, High-precision

1. Introduction

Fitting observed points to geometric shapes is a common problem in science and engineering fields. Among various shapes, circle and ellipse fitting have received much attention from researchers [1, 2, 3, 4, 5], and their fitting methods have been applied in diverse fields, such as robotics [6], engineering measurement [7, 8], and medicine [9, 10]. However, rectangle fitting is equally

*corresponding author.

Email address: yiming.quan@foxmail.com (Yiming Quan)

important for applications in fields such as computer vision [11, 12, 13], medicine [14], and remote sensing [15, 16], where rectangles are widely used as the basic shape for various artifacts. Therefore, it is essential to develop efficient and accurate methods for fitting rectangles to observed data points.

Many studies have attempted to address the problem of finding best-fit rectangular shapes. Some of them applied genetic algorithms (GA) to approximate the polygon [14, 17, 18, 19, 21]. Although GA based methods are effective in solving multi-modal optimization problems, the implementation of GA requires more computation resources and is time-consuming. Liparulo et al. [22] proposed to use fuzzy algorithm to reduce the computational cost of point-to-polygon distance estimation, but their main focus was on recognition rather than fitting shapes. Werman and Keren [20] developed a Bayesian paradigm for parametric and non-parametric fitting of rectangle to noisy data points. Minimum bounding rectangle (MBR), proposed in [23] and [24], has been extensively used for object recognition from LiDAR point clouds [16, 25, 26, 27], images [11, 28, 29, 30, 12], and videos [31, 32]. However, MBR aims to enclose all the points rather than match their distribution. Chaudhuri et al. [33] proposed a rectangle fit method with a bisection of upper and under-estimated rectangles. The iteration scheme of Chaudhuri’s method is based on the computation of rectangle area. However, as pointed out by Yang and Jiang [11], this method may not perform well for discrete and noisy data points, because the area-based fitting metric may not capture the true shape of the data. Another approach to fit rectangle, proposed by Sampath and Shan [34], was to first fit line segments and group them by slopes with parallelism, and then determine the final bounding by least squares with perpendicularity constraints. Building on Chaudhuri’s and Sampath and Shan’s work, Seo et al. [15] proposed a rectangle model with eight parameters (angle and distance parameters for each edge) and used least squares adjustment to fit the model to points, subject to the constraint of perpendicularity between edges. Similarly, Sinnreich [35] employed least squares, but reduced the number of parameters to five, corresponding to the degrees of freedom of a rectangle, and derived a simpler design matrix based on continuous hypotrochoid functions. Stroppa et al. [14] regarded Sinnreich’s algorithm as the most effective method for fitting polygons. However, it was noted that hypotrochoid functions did not fit well at the vertices of polygons [14].

Motivated by these observations, this study introduces a new least squares based rectangle fitting method that aims to overcome the limitations of the

previously discussed methods. The objectives of this paper are to: i) improve the least squares based rectangle fitting algorithm with a more accurate continuous fitness function; ii) evaluate the accuracy of the method in fitting rectangle to clean and noisy data. The rest of this paper is organised as follows. Section 2 presents the new fitness function. Section 3 describes the least squares rectangle fitting algorithm based on the fitness function. Section 4 explains the implementation of the algorithm. Section 5 describes the simulated and real datasets, and reports the testing results and analyses. Section 6 concludes the main finding of this study.

2. A fitness Function for Unit Square

To simplify the rectangle fitting problem, a key step is to find a fitness function for a unit square. We propose a new fitness function for a unit square with coordinates of corners $(0.5, 0.5)$, $(-0.5, 0.5)$, $(-0.5, -0.5)$, $(0.5, -0.5)$, as follows:

$$\begin{aligned} p_x &= \frac{1}{26} \cos \phi (17 - 4 \cos(2\phi) + \frac{0.11}{\cos(4\phi) + 1.08} - \frac{0.22}{\cos(8\phi) + 2}) \\ p_y &= \frac{1}{26} \sin \phi (17 + 4 \cos(2\phi) + \frac{0.11}{\cos(4\phi) + 1.08} - \frac{0.22}{\cos(8\phi) + 2}) \end{aligned} \quad (1)$$

Eqs. (1), which consist of sine and cosine functions, approximate the unit square precisely with an angle parameter, ϕ . This function enables the implementation of a simple and computationally efficient least squares algorithm to fit rectangles of any position and size.

3. Rectangle Fitting by Least Squares

Multiplying the unit square by a scaling matrix $\mathbf{M}=\text{diag}(m_x, m_y)$ to stretch it in x and y coordinates, and then applying a rotation matrix \mathbf{R} corresponding to a counterclockwise rotation angle α and a translation vector $\mathbf{T}=[x_c, y_c]^T$, any rectangle in the plane can be fitted. Therefore, a rectangle can be defined by a vector of five parameters given by:

$$\mathbf{V} = [x_c \ y_c \ m_x \ m_y \ \alpha]^T \quad (2)$$

where (x_c, y_c) is the centre of the rectangle, m_x and m_y are the lengths of edges, and α is the orientation of the rectangle. Based on the fitness function

for unit square, we can find a rectangle by minimizing the function for data points given by:

$$\begin{aligned}\mathbf{L} &= [\mathbf{L}_1 \quad \mathbf{L}_2 \quad \cdots \quad \mathbf{L}_n]^T, \\ \mathbf{L}_i &= \mathbf{R}^T(\mathbf{X}_i - \mathbf{T}) - \mathbf{M} \cdot \mathbf{P}_i \\ &= \begin{bmatrix} \cos \alpha & \sin \alpha \\ -\sin \alpha & \cos \alpha \end{bmatrix} \begin{bmatrix} x_i - x_c \\ y_i - y_c \end{bmatrix} - \begin{bmatrix} m_x p_x \\ m_y p_y \end{bmatrix}\end{aligned}\tag{3}$$

where $\mathbf{X}_i = [x_i, y_i]^T$ are the coordinates of data points, and $\mathbf{P}_i = [p_x, p_y]^T$ is the unit square defined in Eqs. (1). A numerical solution of ϕ can be calculated for each data point. We omit the tedious algebraic computations and present the final result as follows:

$$\begin{aligned}\phi &= \text{sgn}(\tan \theta) \arccos(\sqrt{1.75 - 2.5k - (q_1 + q_2)^{1/3} - (q_1 - q_2)^{1/3}}) \\ &\quad + \text{sgn}(\sin \theta) \text{stp}(\cos \theta) \pi\end{aligned}\tag{4}$$

where

$$\theta = \arctan((y_i - y_c)/(x_i - x_c)) - \alpha\tag{4a}$$

$$\begin{aligned}q_1 &= p_1(k - 0.5)^3 - p_2(k - 0.5), \\ q_2 &= p_3 \sqrt{(k^2 - k)(k - k^2 - p_4)}\end{aligned}\tag{4b}$$

the squared aspect ratio is defined as $h = m_y^2/m_x^2$ and notation $k = h/(h + \tan^2 \theta)$, $p_1=15.625$, $p_2=5.246102$, $p_3=8.399833$, $p_4=0.278687$ is used for brevity. $\text{sgn}(\cdot)$ is the sign function, and $\text{stp}(\cdot)$ is a step function defined as:

$$\text{stp}(x) = \begin{cases} 0; & \text{if } x \geq 0 \\ 1; & \text{if } x < 0 \end{cases}\tag{4c}$$

The standard Gauss-Newton method is used to minimise \mathbf{L} :

$$\mathbf{g} = -(\mathbf{A}^T \mathbf{A})^{-1} \mathbf{A}^T \mathbf{L}\tag{5a}$$

$$\mathbf{V} := \mathbf{V} + \mathbf{g}\tag{5b}$$

where \mathbf{A} is partial derivatives of \mathbf{L} given by:

$$\begin{aligned}\mathbf{A} &= [\mathbf{A}_1 \quad \mathbf{A}_2 \quad \cdots \quad \mathbf{A}_n]^T, \\ \mathbf{A}_i &= \begin{bmatrix} \frac{\partial \mathbf{L}_i}{\partial x_c} & \frac{\partial \mathbf{L}_i}{\partial y_c} & \frac{\partial \mathbf{L}_i}{\partial m_x} & \frac{\partial \mathbf{L}_i}{\partial m_y} & \frac{\partial \mathbf{L}_i}{\partial \alpha} \end{bmatrix}\end{aligned}\quad (6)$$

From Eq. (3), we can have:

$$\begin{aligned}\frac{\partial \mathbf{L}_i}{\partial x_c} &= \begin{bmatrix} -\cos \alpha \\ \sin \alpha \end{bmatrix} - \begin{bmatrix} m_x \frac{\partial p_x}{\partial \phi} \frac{\partial \phi}{\partial \theta} \frac{\partial \theta}{\partial x_c} \\ m_y \frac{\partial p_y}{\partial \phi} \frac{\partial \phi}{\partial \theta} \frac{\partial \theta}{\partial x_c} \end{bmatrix}, \\ \frac{\partial \mathbf{L}_i}{\partial y_c} &= \begin{bmatrix} -\sin \alpha \\ -\cos \alpha \end{bmatrix} - \begin{bmatrix} m_x \frac{\partial p_x}{\partial \phi} \frac{\partial \phi}{\partial \theta} \frac{\partial \theta}{\partial y_c} \\ m_y \frac{\partial p_y}{\partial \phi} \frac{\partial \phi}{\partial \theta} \frac{\partial \theta}{\partial y_c} \end{bmatrix}\end{aligned}\quad (6a)$$

$$\frac{\partial \mathbf{L}_i}{\partial m_x} = - \begin{bmatrix} p_x + m_x \frac{\partial p_x}{\partial \phi} \frac{\partial \phi}{\partial m_x} \\ m_y \frac{\partial p_y}{\partial \phi} \frac{\partial \phi}{\partial m_x} \end{bmatrix}, \quad \frac{\partial \mathbf{L}_i}{\partial m_y} = - \begin{bmatrix} m_x \frac{\partial p_x}{\partial \phi} \frac{\partial \phi}{\partial m_y} \\ p_y + m_y \frac{\partial p_y}{\partial \phi} \frac{\partial \phi}{\partial m_y} \end{bmatrix}\quad (6b)$$

$$\frac{\partial \mathbf{L}_i}{\partial \alpha} = \begin{bmatrix} -\sin \alpha (x_i - x_c) + \cos \alpha (y_i - y_c) \\ -\cos \alpha (x_i - x_c) - \sin \alpha (y_i - y_c) \end{bmatrix} - \begin{bmatrix} m_x \frac{\partial p_x}{\partial \phi} \frac{\partial \phi}{\partial \alpha} \\ m_y \frac{\partial p_y}{\partial \phi} \frac{\partial \phi}{\partial \alpha} \end{bmatrix}\quad (6c)$$

The partial derivatives of p_x and p_y with respect to ϕ in Eqs. (6a), (6b), and (6c) are given by:

$$\begin{aligned}\frac{\partial p_x}{\partial \phi} &= \frac{\sin \phi (12 \cos(2\phi) - 9)}{26} + \dot{\epsilon}_x, \\ \frac{\partial p_y}{\partial \phi} &= \frac{\cos \phi (12 \cos(2\phi) + 9)}{26} + \dot{\epsilon}_y\end{aligned}\quad (7a)$$

where $\dot{\epsilon}_x$ and $\dot{\epsilon}_y$ are the partial derivatives of terms with 4ϕ and 8ϕ in Eqs. (1). Since the terms with 4ϕ and 8ϕ and their derivatives are sufficiently small compared to other terms, we found it does not affect the convergence of iteration if they are assumed to be zero.

The other partial derivatives in Eqs. (6a), (6b), and (6c) are:

$$\frac{\partial \phi}{\partial \theta} = -\frac{\partial \phi}{\partial \alpha} = \frac{\partial \phi}{\partial k} \frac{\partial k}{\partial \theta}\quad (7b)$$

$$\begin{aligned}\frac{\partial \theta}{\partial x_c} &= \frac{y_i - y_c}{(x_i - x_c)^2 + (y_i - y_c)^2}, \\ \frac{\partial \theta}{\partial y_c} &= \frac{-x_i + x_c}{(x_i - x_c)^2 + (y_i - y_c)^2}\end{aligned}\tag{7c}$$

$$\frac{\partial \phi}{\partial m_x} = \frac{\partial \phi}{\partial k} \frac{\partial k}{\partial m_x}, \quad \frac{\partial \phi}{\partial m_y} = \frac{\partial \phi}{\partial k} \frac{\partial k}{\partial m_y}\tag{7d}$$

where we use notation $v = \sqrt{1.75 - 2.5k - (q_1 + q_2)^{1/3} - (q_1 - q_2)^{1/3}}$, $t = \tan^2 \theta$, and gives:

$$\frac{\partial \phi}{\partial k} = \text{sgn}(\tan \theta) \frac{7.5 + \frac{\partial(q_1+q_2)}{\partial k}(q_1 + q_2)^{-2/3} + \frac{\partial(q_1-q_2)}{\partial k}(q_1 - q_2)^{-2/3}}{6\sqrt{v(1-v)}}\tag{8a}$$

$$\frac{\partial k}{\partial \theta} = \frac{2h(t+1)\tan \theta}{(t+h)^2}\tag{8b}$$

$$\frac{\partial k}{\partial m_x} = -\frac{2ht}{m_x(t+h)^2}, \quad \frac{\partial k}{\partial m_y} = \frac{2ht}{m_y(t+h)^2}\tag{8c}$$

in Eq. (8a), we can calculate $\frac{\partial(q_1+q_2)}{\partial k}$ and $\frac{\partial(q_1-q_2)}{\partial k}$ from q_1 and q_2 defined in Eqs. (4b), given by:

$$\frac{\partial q_1}{\partial k} = 3p_1(k-0.5)^2 - p_2, \quad \frac{\partial q_2}{\partial k} = -\frac{p_3(2k-1)(p_4+2k(k-1))}{2\sqrt{-k(k-1)(p_4+k(k-1))}}\tag{8d}$$

Moreover, if the fitted rectangle is a square, then the number of parameters in Eq. (2) is reduced to four, as $m_x = m_y = m$, similar modifications apply to other equations in this section. The iteration stops when the norm of the step of \mathbf{V} gets smaller than 10^{-6} in this study.

4. Algorithm Implementation

Before applying the proposed method, the data should be preprocessed with the following steps, which are analogous to the data preprocessing in circle fitting [2]:

- a) Centre the data points by applying translation: $x'_i = x_i - \bar{x}$ and $y'_i = y_i - \bar{y}$, where \bar{x} and \bar{y} are sample means of x_i and y_i , respectively.
- b) Scale data by dividing x'_i and y'_i by the root mean squared distance, d_{rms} , of the translated data points from the origin.
- c) Apply singular value decomposition (SVD) to the translated and scaled data points $\mathbf{u}\mathbf{v}^T = \mathbf{X}'$, use the angle of the singular vector as the initial estimate of α .

Applying these steps can reduce rounding error and mis-convergence in iteration. We can start the search of the parameters (x_c, y_c, m_x, m_y) at $(0, 0, 1, 1)$ with the calculated initial value of α . The converged parameters after iteration are then scaled and translated back by:

$$\begin{aligned} x_c &\leftarrow x_c d_{\text{rms}} + \bar{x}, y_c \leftarrow y_c d_{\text{rms}} + \bar{y}, \\ m_x &\leftarrow m_x d_{\text{rms}}, m_y \leftarrow m_y d_{\text{rms}} \end{aligned} \tag{9}$$

Algorithm 1 shows the procedures of data preprocessing and iterative least squares minimisation.

Algorithm 1 Proposed Rectanlge Fit Algorithm

- 1: **procedure** DATA PREPROCESSING
 - 2: **for** each (x_i, y_i) in \mathbf{X} **do**
 - $x_i \leftarrow (x_i - \bar{x})/d_{\text{rms}}$
 - $y_i \leftarrow (y_i - \bar{y})/d_{\text{rms}}$
 - 3: Compute α_0 by $\mathbf{u}, \mathbf{s}, \mathbf{v}^T := \text{svd}(\mathbf{X})$
 $\alpha_0 := \arctan(\mathbf{v}^T)$
 - 4: **procedure** ITERATIVE LEAST SQUARES MINIMIZATION
 - 5: Initialise $\mathbf{V} := [0, 0, 1, 1, \alpha_0]^T$, $\epsilon := 10^{-6}$
 - 6: **while** not converged **do**
 - 7: Compute ϕ by Eq. (4)
 - 8: Compute \mathbf{L} by Eq. (3)
 - 9: Compute \mathbf{A} by Eq. (6)
 - 10: Compute \mathbf{g} by Eq. (5a)
 - 11: **if** $\|\mathbf{g}\| < \epsilon\|\mathbf{V}\|$ **then** break
 - 12: **else**
 - 13: $\mathbf{V} \leftarrow \mathbf{V} + \mathbf{g}$
 - 14: restore (x_c, y_c, m_x, m_y) in estimated \mathbf{V} by Eqs. (9)
-

5. Validation

The proposed method are validated with simulated and real data, and compared with the method proposed by Sinnreich [35] in terms of accuracy. Section 5.1 describes the test datasets used in this study and Section 5.2 presents the results and analyses. We uses root-mean-square error (RMSE) to evaluate fitting accuracy of the proposed fitting methods.

5.1. Data Description

Four datasets were used to validate the proposed method. Dataset A contained 40 clean points uniformly distributed on a unit square as defined in Section 2. Dataset A was designed to quantitatively test the systematic error of the proposed unit square fitness function, i.e. Eqs. (1), compared with the hypotrochoid function proposed by Sinnreich [35]. Dataset B contained 10 clean points sparsely distributed on a rectangle. The coordinate pairs of the 10 points are shown in Table 2. We used Dataset B to evaluate the performance of the proposed when the number of points was small. Dataset C contained a dense point cloud affected by Gaussian Noise. Dataset D contained sliced point cloud of a building collected using aerial photogrammetry as shown in Fig. 1. The parameters of rectangle in Dataset D were computed using the planar coordinates of the four corner points of the building. The true coordinates of the building corners came from the as-built drawing based on total station survey.

Table 1: Coordinates of ten points in Dataset B

X	9.1641	7.9641	6.8094	3.3453	1.3692
Y	7.5196	9.5981	8.9314	6.9314	5.0207
X	2.3692	3.3692	8.0774	9.8094	10.0641
Y	3.2887	1.5566	2.7353	3.7353	5.9608

5.2. Result

As mentioned in the previous subsection, we used Dataset A to assess the accuracy of unit square fitness function. Table 2 shows the estimated parameters and RMSE of fitting points. The results indicate that for a unit square, the proposed method can achieve an accuracy of 0.001, while the accuracy of Sinnreich’s fit is 0.016. The main source of error for Sinnreich’s

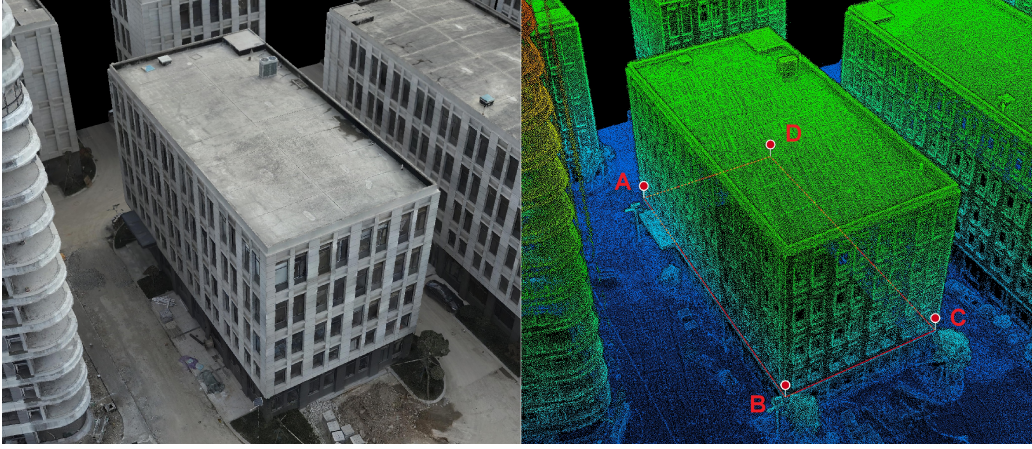


Figure 1: 3D model(left) and point cloud(right) of the building from aerial photogrammetry. Dataset D is the sliced point cloud near Plane ABCD.

fit is the overestimation of edge length caused by increasing error close to the vertices. Fig. 2 shows the comparison of the proposed fit and Sinnreich’s fit on Dataset A with ground truth points. Fig. 2 illustrates that Sinnreich’s fit exhibits a slight outward deviation from the square except near the vertices, where it curves inward. In contrast, the proposed fit shows closer proximity to the unit square, especially in capturing the vertices.

Table 2: Fitting result of Dataset A and RMSE of fitting points

Parameters	Ground truth	Sinnreich fit	proposed fit
x_c	0	0.000	0.000
y_c	0	0.000	0.000
m_x	1	1.011	1.001
m_y	1	1.011	1.001
α/deg	0	0.000	0.000
RMSE		0.016	0.001

Tables 3, 4, and 5 show the estimated parameters and RMSE of fitting points of Datasets B, C, and D, respectively. The results of simulated tests indicate that the proposed method outperforms Sinnreich’s method, with about 93% lower RMSE, in the case of sparsely distributed points without noise, and with about 14% lower RMSE, in the case of dense point cloud

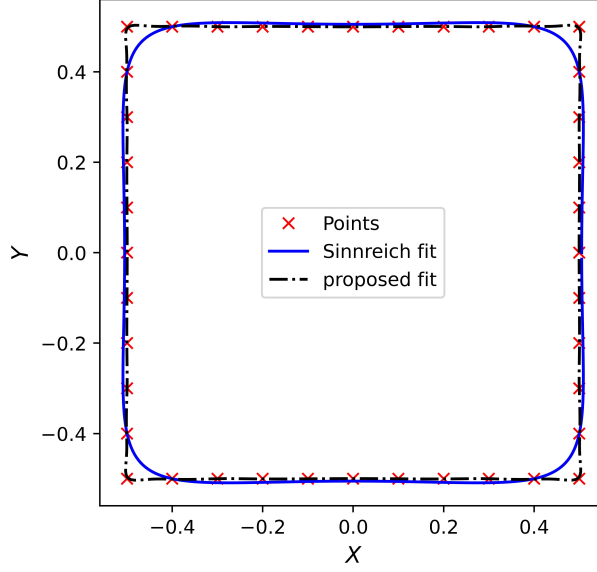


Figure 2: Comparison of unit square fits on Dataset A with ground truth points

with Gaussian noise. The test result of real data indicates that the proposed method can achieve centimetre level accuracy, while Sinnreich’s method has decimetre level accuracy in Dataset D. From Tables 3 to 5, we can observe that Sinnreich fit overestimates the edge length in all tests as well as in Dataset A. Fig. 3 illustrates the comparison of the proposed fit and Sinnreich’s fit on Datasets B, C, and D with data points. From Fig. 3, the proposed fit shows closer proximity to the rectangle in Datasets B and D, which are clean and less noisy.

Table 3: Fitting result of Dataset B and RMSE of fitting points			
Parameters	Ground truth	Sinnreich fit	proposed fit
x_c	6	6.016	6.001
y_c	5	5.041	5.003
m_x	8	8.054	8.008
m_y	6	6.062	6.000
α/deg	30	30.02	29.98
RMSE		0.107	0.008

Table 4: Fitting result of Dataset C and RMSE of fitting points

Parameters	Ground truth	Sinnreich fit	proposed fit
x_c	-7	-7.009	-6.964
y_c	11	11.040	10.987
m_x	37	37.255	36.926
m_y	17	17.107	16.898
α/deg	131	130.85	130.85
RMSE		0.629	0.554

Table 5: Fitting result of Dataset D and RMSE of fitting points

Parameters	Ground truth	Sinnreich fit	proposed fit
x_c/m	295595.930	295595.921	295595.959
y_c/m	95593.943	95593.871	95593.902
m_x/m	33.100	33.422	33.102
m_y/m	16.685	17.137	16.733
α/deg	155.77	155.20	155.84
RMSE/m		0.461	0.087

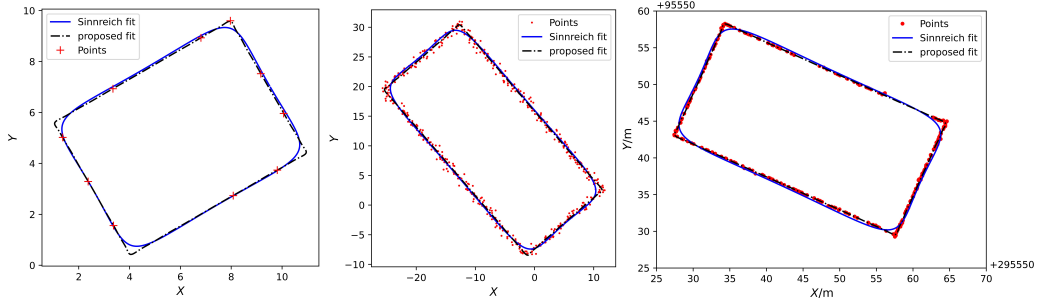


Figure 3: Comparison of rectangle fits on Datasets B (left), C(middle), and D(right)

Fig. 4 shows the convergence of the parameter estimation of the proposed method with Datasets B, C, and D. The parameters shown in the right-hand-side column were restored using Eqs. (9) as the data preprocessing described in Section 4 is used before the fit. Fig. 4 indicates that the least squares estimation converges in fewer than 10 iterations with the given datasets.

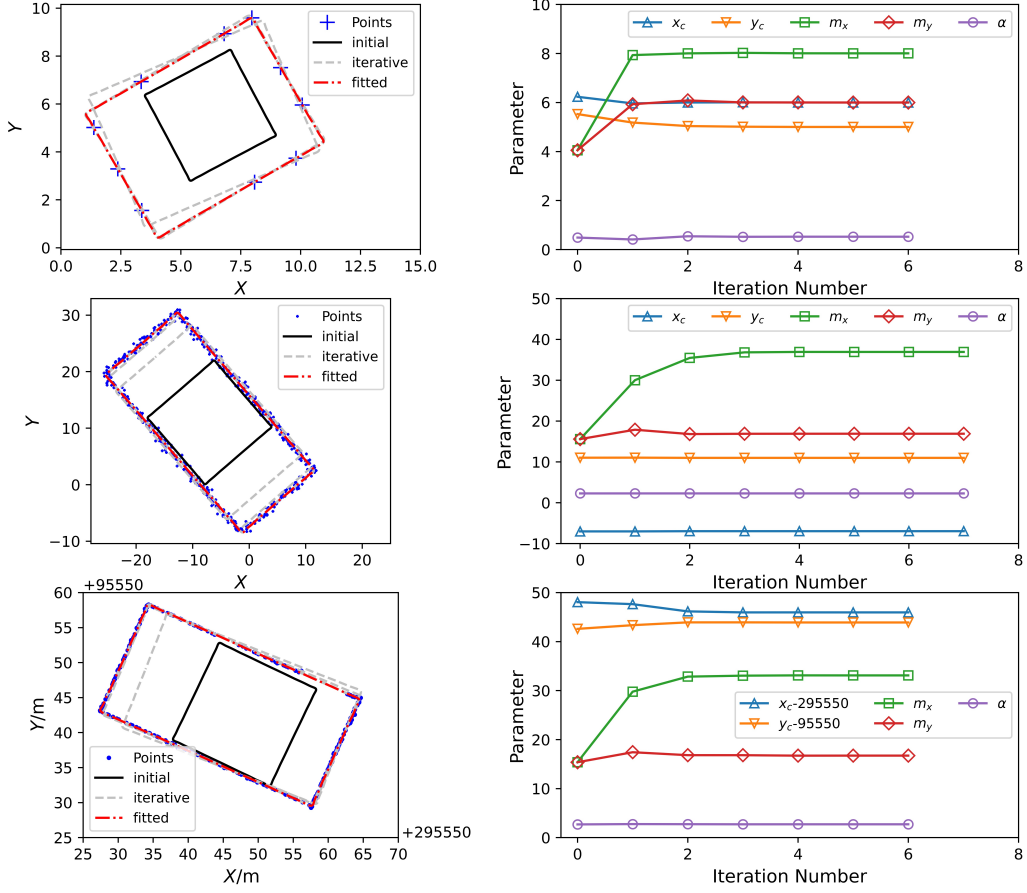


Figure 4: Fitting processing and convergence of parameters with Dataset B(top), Dataset C(centre), and Dataset D(bottom)

6. Conclusions

This work has presented a new approach for efficient and accurate rectangle fitting to data points based on a continuous fitness function for a unit square. We tested the proposed method with clean and noisy simulated data as well as real point cloud data from aerial photogrammetry. The proposed method are compared with the existing method in the literature. The results show that the proposed method achieved a better accuracy with an about 93% lower root-mean-square error in clean simulated datasets, and 81% improvements in noisy and real point clouds, respectively. The proposed method also converged fast, requiring fewer than 10 iterations.

Acknowledgement

This work was supported by 2021 Science and Technology Projects of Zhejiang Provincial Department of Natural; Ningbo Tianyi Design Research of Surveying and Mapping co. Ltd.

References

- [1] F. Mai, Y.S. Hung, H. Zhong, W. F. Sze, A hierarchical approach for fast and robust ellipse extraction, *Pattern Recognit.* 41 (8) (2008) 2512-2524, doi:10.1016/j.patcog.2008.01.027.
- [2] H. Abdul-Rahman, N. Chernov, Fast and numerically stable circle fit, *J Math Imaging Vis* 116 (2014) 289–295, doi:10.1007/s10851-013-0461-4.
- [3] D.K. Prasad, M.K. Leung, C. Quek, ElliFit: An unconstrained, non iterative, least squares based geometric ellipse fitting method, *Pattern Recognit.* 46 (5) (2013) 1449-1465, doi: 10.1016/j.patcog.2012.11.007.
- [4] T. Wang, Z. Shi, B. Yu, A parameterized geometric fitting method for ellipse, *Pattern Recognit.* 116 (2021) 107934, doi:10.1016/j.patcog.2021.107934.
- [5] R. Maalek, D.D. Lichti, New confocal hyperbola-based ellipse fitting with applications to estimating parameters of mechanical pipes from point clouds, *Pattern Recognit.* 116 (2021) 107948, doi:10.1016/j.patcog.2021.107948.
- [6] H. Dong, E. Asadi, G. Sun, D.K. Prasad, I.-M. Chen, Real-time robotic manipulation of cylindrical objects in dynamic scenarios through elliptic shape primitives, *IEEE Trans. Robot.* (2018) 1–19, doi:10.1109/tro.2018.2868804.
- [7] Y. Quan, L. Lau, Development of a trajectory constrained rotating arm rig for testing GNSS kinematic positioning, *Measurement* 140 (2019) 479-485, doi:10.1016/j.measurement.2019.04.013.
- [8] Z. Lu, B. Liu, K. Zhang, H. Lin and Y. Zhang, A Method for Measuring the Inclination of Forgings Based on an Improved Optimization Algorithm for Fitting Ellipses, *IEEE Trans. Instrum. Meas.* 72 (2023) 1-11, doi: 10.1109/TIM.2022.3221761.
- [9] J. Li, Y. Wang, B. Lei, J.-Z. Cheng, J. Qin, T. Wang, S. Li, D. Ni, Automatic fetal head circumference measurement in ultrasound using random forest and fast ellipse fitting, *IEEE J. Biomed. Health*, 22 (1) (2018) 215-223, doi: 10.1109/JBHI.2017.2703890.

- [10] R. Ranjbarzadeh, S.B. Saadi, Automated liver and tumor segmentation based on concave and convex points using fuzzy c-means and mean shift clustering, *Measurement* 150 (2020) 107086, doi: 10.1016/j.measurement.2019.107086.
- [11] J. Yang, Z. Jiang, Rectangle fitting via quadratic programming, in: 2015 IEEE 17th International Workshop on Multimedia Signal Processing, Xiamen, China, 2015, pp. 1-6, doi: 10.1109/MMSP.2015.7340875.
- [12] Z. Liu, H. Wang, L. Weng, Y. Yang, Ship rotated bounding box space for ship extraction from high-resolution optical satellite images with complex backgrounds, *IEEE Geosci. Remote Sens. Lett.* 13 (8) (2016) 1074–1078, doi: 10.1109/LGRS.2016.2565705.
- [13] J. -C. Bazin, I. Kweon, C. Démonceaux, P. Vasseur, Rectangle extraction in catadioptric images, in: IEEE 11th International Conference on Computer Vision, Rio de Janeiro, Brazil, 2007, pp. 1-7, doi: 10.1109/ICCV.2007.4409208.
- [14] F. Stroppa, C. Loconsole, A. Frisoli, Convex polygon fitting in robot-based neurorehabilitation, *Appl. Soft Comput. J.* 68 (2018) 609-625, doi:10.1016/j.asoc.2018.04.013.
- [15] S. Seo, J. Lee, Y. Kim, Extraction of boundaries of rooftop fenced buildings from airborne laser scanning data using rectangle models, *IEEE Geosci. Remote Sens. Lett.* 11 (2) (2014) 404-408, doi: 10.1109/LGRS.2013.2263575.
- [16] M. Feng, T. Zhang, S. Li, G. Jin, Y. Xia, An improved minimum bounding rectangle algorithm for regularized building boundary extraction from aerial LiDAR point clouds with partial occlusions, *Int. J. Remote Sens.* 41 (2) (2020) 300-319, doi: 10.1080/01431161.2019.1641245.
- [17] P. Yin, A new method for polygonal approximation using genetic algorithms, *Pattern Recognit. Lett.* 19 (1998) 1017-1026, doi:10.1016/s0167-8655(98)00082-8.
- [18] P. Yin, Genetic algorithms for polygonal approximation of digital curves, *Int. J. Pattern Recognit. Artif. Intell.* 13 (7) (1999) 1061-1082, doi:10.1142/S0218001499000598.

- [19] Y. Tsai, Fast polygonal approximation based on genetic algorithms, in: 5th IEEE/ACIS International Conference on Computer and Information Science and 1st IEEE/ACIS International Workshop on Component-Based Software Engineering, Software Architecture and Reuse, 2006, pp. 322–326, doi:10.1109/icis-comsar.2006.39.
- [20] M. Werman, D. Keren, A Bayesian method for fitting parametric and non-parametric models to noisy data, *IEEE Trans. Pattern Analysis Mach. Intell.* 23 (5) (2001) 528–534, doi: 10.1109/34.922710.
- [21] Z. Liu, J. Watson, A. Allen, A polygonal approximation of shape boundaries of marine plankton based-on genetic algorithms, *J. Vis. Commun. Image Represent.* 41 (2016) 305–313, doi:10.1016/j.jvcir.2016.10.010.
- [22] L. Liparulo, A. Proietti, M. Panella, Fuzzy membership functions based on point-to-polygon distance evaluation, in: 2013 IEEE International Conference on Fuzzy Systems, 2013, pp. 1–8, doi:10.1109/fuzz-ieee.2013.6622449.
- [23] H. Freeman and R. Shapira, Determining the minimum-area encasing rectangle for an arbitrary closed curve, *Commun. ACM*, 18 (7) (1975) 409–413, doi:10.1145/360881.360919.
- [24] D. Chaudhuri and A. Samal, A simple method for fitting of bounding rectangle to closed regions, *Pattern Recognit.* 40 (7) (2007) 1981–1989, doi:10.1016/j.patcog.2006.08.003.
- [25] E. Kwak, M. Al-Durgham, A. Habib, Automatic 3D building model generation from lidar and image data using sequential minimum bounding rectangle, *Int. Arch. Photogramm. Remote Sens. Spatial Inf. Sci.*, XXXIX-B3 (2012) 285–290, doi:10.5194/isprsarchives-XXXIX-B3-285-2012.
- [26] E. Kwak, A. Habib, Automatic representation and reconstruction of DBM from LiDAR data using Recursive Minimum Bounding Rectangle, *ISPRS J Photogramm. Remote Sens.* 93 (2014) 171–191, doi:10.1016/j.isprsjprs.2013.10.003.
- [27] M. Kabolizade, H. Ebadi, A. Mohammadzadeh, Design and implementation of an algorithm for automatic 3D reconstruction of building models

- using genetic algorithm, *Int. J. Appl. Earth Obs. Geoinf.* 19 (2012) 104-114, doi:10.1016/j.jag.2012.05.006.
- [28] Y. Wang, L. Wang, H. Lu, Y. He, Segmentation based rotated bounding boxes prediction and image synthesizing for object detection of high resolution aerial images, *Neurocomputing*, 388 (2020) 202-211, doi:10.1016/j.neucom.2020.01.039.
 - [29] G.-S. Xia, X. Bai, J. Ding, Z. Zhu, S. Belongie, J. Luo, M. Datcu, M. Pelillo, L. Zhang, DOTA: a large-scale dataset for object detection in aerial images, in: *Proceedings of the IEEE Conference on Computer Vision and Pattern Recognition (CVPR)*, 2018.
 - [30] J. Ding, N. Xue, Y. Long, G.-S. Xia, Q. Lu, Learning RoI transformer for detecting oriented objects in aerial images, in: *Proceedings of the IEEE Conference on Computer Vision and Pattern Recognition (CVPR)*, 2019.
 - [31] A. Edgcomb, F. Vahid, Automated fall detection on privacy-enhanced video, in: *2012 Annual International Conference of the IEEE Engineering in Medicine and Biology Society*, San Diego, CA, USA, 2012, pp. 252-255, doi: 10.1109/EMBC.2012.6345917.
 - [32] W.-C. Hu, C.-H. Chen, T.-Y. Chen, D.-Y. Huang, Z.-C. Wu, Moving object detection and tracking from video captured by moving camera, *J. Vis. Commun. Image Represent.* 30 (2015) 164-180, doi:10.1016/j.jvcir.2015.03.003.
 - [33] D. Chaudhuri, N. K. Kushwaha, I. Sharif, A. Samal, Finding best-fitted rectangle for regions using a bisection method, *Mach. Vis. Appl.* 23 (6) (2011) 1263-1271, doi:10.1007/s00138-011-0348-6.
 - [34] A. Sampath, J. Shan, Building boundary tracing and regularization from airborne lidar point clouds, *Photogramm. Eng. Remote Sens.* 73 (7) (2007) 805-812, doi:10.14358/PERS.73.7.805.
 - [35] J. Sinnreich, Least-squares fitting of polygons, *Pattern Recognit. Image Analysis* 26 (2) (2016) 343-349, doi:10.1134/S10546618160202180.